Microfluidic Separation System for Magnetic Beads

F. Wittbracht*, A. Weddemann, A. Auge and A. Hütten
Bielefeld University, Department of Physics
*Universitätsstr. 25, 33615 Bielefeld, Germany, fwittbra@physik.uni-bielefeld.de

Abstract: Lab-on-a-chip technologies and the μTAS have gained importance in recent years. The integration of all functions and components needed for the analysis of a sample in a microfluidic system has to be achieved. Magnetic materials are widely used in these systems for various applications such as magnetohydrodynamic pumps and valves. Especially, in terms of separation and detection of biological samples magnetic materials are suitable.
In this work a microfluidic separation system for magnetic beads was experimentally realized according to theoretical simulations. The manipulation of magnetic beads is achieved by magnetic gradient fields resulting from conducting lines near the microfluidic channel. Experimental and calculation results are compared with each other.

Keywords: Microfluidic device, magnetic beads, separation mechanism

1. Introduction

The analysis of particles with a permanent magnetic moment, so called magnetic beads, is of growing interest due to their wide field of applications [1]. As they feel a force in an inhomogenous magnetic field, it is possible to control their motion using a combination of hydrodynamic and electromagnetic forces [2].

This makes them suitable for biomedical applications such as cancer treatment. Binding medical agents to the magnetic beads, the agents themselves can be manipulated by external fields. Thus, their movement can be restricted to the affected area, increasing the drug efficiency and reducing severe side effects [3].

In this work, we investigate the possibility to manipulate the motion of the particles with different magnetic moments in a special microfluidic structure. By the combined use of magnetic and hydrodynamic forces we will suggest a way to separate particles in respect to different properties.

2. Governing equations

2.1 Fluid dynamics

To understand the behaviour of particles in different fluid channels it is first necessary to understand the dynamics of the liquid itself. The theoretical description in this case bases on two principles. On the one hand, this is the principle of mass conservation, leading to the equation of continuity

$$\nabla \boldsymbol{u} = 0\,, \tag{2.1}$$

where $\boldsymbol{u}$ is the velocity of the fluid. On the other hand, it is assumed that the total momentum is conserved. Together with (2.1) this gives the Navier-Stokes equation for incompressible fluids

$$\frac{\partial \boldsymbol{u}}{\partial t} + (\boldsymbol{u}\nabla)\boldsymbol{u} = -\frac{\nabla p}{\rho} + \frac{\eta}{\rho}\Delta \boldsymbol{u} + \boldsymbol{f}\,, \tag{2.2}$$

where p denotes the pressure, η and ρ are the viscosity and the density of the fluid, respectively, and $\boldsymbol{f}$ is an external force density. For the calculations we will expect the carrier liquid to be water at room temperature, therefore, we have $\eta = 1.002 mPa\,s$ and $\rho = 998.2 kg/m^3$.
The resulting velocity profile for the systems analysed here are always in the regime of laminar flow. This means, there is no time dependence of $\boldsymbol{u}$, and the streamlines are parallel to each other. This is due to a Reynolds number

$$Re = \frac{LU\rho}{\eta} \tag{2.3}$$

much smaller than 1. U and L are characteristic size scales: U corresponds to the characteristic velocity of the fluid profile, while L is the typical length scale.

In this low Reynolds number regime, the force $\boldsymbol{F}$ on a spherical object of radius r suspended in a liquid is given by Stokes drag law

$$\boldsymbol{F} = 6\pi\eta r(\boldsymbol{u} - \boldsymbol{v}), \tag{2.4}$$

where $\boldsymbol{v}$ is the velocity of the sphere.

2.2 Particle diffusion

Small particles suspended in a liquid left to themselves will move because of their thermal energy. A given concentration distribution of particles will not stay constant over time, but change according to the equation

$$\frac{\partial c}{\partial t} = -\nabla \cdot \boldsymbol{j}, \tag{2.7a}$$

with $$\boldsymbol{j} = -D\nabla c + c\boldsymbol{u}, \tag{2.7b}$$

where D is the diffusion constant. In case of spherical particles of radius r it can be written as

$$D = \frac{k_B T}{6\pi\eta r}, \tag{2.8}$$

where T is the temperature and k_B is the Boltzman constant. The two terms in the flux $\boldsymbol{j}$ correspond to diffusive and convective particle movement, respectively. Diffusive effects can be neglected if the particle size is big enough (about several hundred nanometer) but have to be taken into account for beads at the range of $100nm$ and below.

2.3 Electromagnetics

Particles with a magnetic moment $\boldsymbol{m}$ interact with electromagnetic fields $\boldsymbol{B}$. Usually it is not easy to create magnetic fields suitable for certain applications. However, it is well known that electric current densities $\boldsymbol{J}$ create magnetic fields, given by the Maxwell equations

$$\nabla \times \boldsymbol{B} = \boldsymbol{J} \tag{2.9a}$$

and $$\nabla \cdot \boldsymbol{B} = 0, \tag{2.9b}$$

where the magnetic field $\boldsymbol{B}$ may be written with the help of a vector potential $\boldsymbol{A}$ as

$$\boldsymbol{B} = \nabla \times \boldsymbol{A}. \tag{2.9c}$$

2.4 Particle movement

Apart from hydrodynamic forces there are other effects influencing the particles. We will especially be interested in magnetic forces caused by inhomogenous external fields acting on the magnetic moment of the particles. Combining (2.4) with a magnetic force $\boldsymbol{F}_{mag}$ the velocity of small spherical particles is given by

$$\boldsymbol{v} = \boldsymbol{u} + \frac{\boldsymbol{F}_{mag}}{6\pi\eta r}. \tag{2.5}$$

A particle of given magnetic moment $\boldsymbol{m}$ aligns with an external magnetic field on the one hand. Furthermore, it feels a force within an inhomogenous field $\boldsymbol{B}$, given by

$$\boldsymbol{F}_{mag} = (\boldsymbol{m}\nabla)\boldsymbol{B}. \tag{2.6a}$$

To simplify the model we expect particles to be superparamagnetic, i.e. their magnetic moment instantaneously aligns with an external magnetic field. In this case equation (2.6a) may be written in the form

$$\boldsymbol{F}_{mag} = \frac{|\boldsymbol{m}|}{2|\boldsymbol{B}|}\nabla \boldsymbol{B}^2. \tag{2.6b}$$

Gravity and buoyancy acting on the objects are much smaller than the effects mentioned above, why we will neglect these in the following analysis. Furthermore, we make the assumption that particle-particle interactions resulting from magnetic dipole forces can be neglected. For the experimental setups this assumption will be met, if the particle concentration is sufficiently small.

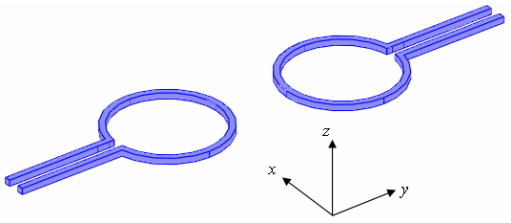

Fig. 1: Schematic drawing of the wire geometry used for the field creation. For the simulations, a square cross section of side length $10\mu m$ and an outer ring radius of $100\mu m$ are assumed. The centres of the rings have a distance of $440\mu m$.

3. Magnetic field creation

To manipulate the magnetic microparticles in our application two different magnetic field contributions are needed. On the one hand, a homogenous magnetic field pointing in z-direction (perpendicular to the mircofluidic structure) is used, which is chosen strong enough to saturate the magnetic particles. From (2.6a) we therefore conclude that the force acting on the particles in an inhomogenous magnetic field is given by

$$F_{i,mag} = m_z \partial_z B_i \qquad (3.1)$$

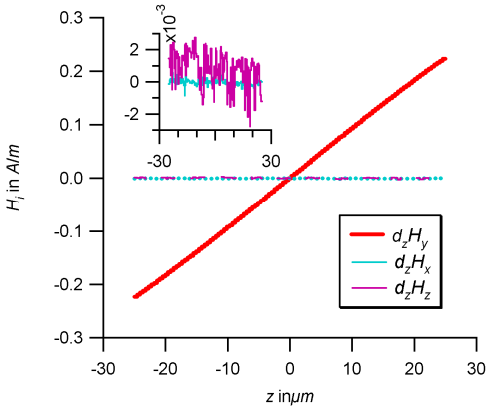

Fig. 2: Resulting magnetic field derivatives for the geometry shown in Fig. 1, if a current of $1mA$ flows parallel through both wires. Apart from the component needed for the separation, all contributions are at the scale of numeric noise.

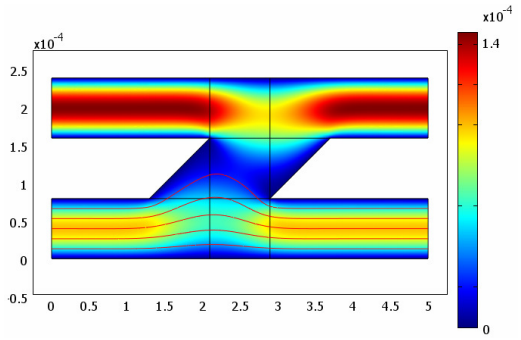

Fig. 3: Microfluidic structure entrances (left) and exits (right) have a width of $80\mu m$. The velocity at the upper entrance is chosen as 1.4551 times the velocity at the lower entrance. Thus, it is ensured that there is no volume flux from the lower to the upper part of the geometry, what is indicated by the streamline plot.

Thus, if the particle flow direction is supposed to be parallel with the x-axis, and a force in y-direction is to be applied, the inhomogenous field contribution has to be chosen, to have a high derivative $\partial_z B_y$. This is achieved with the wire geometry shown in Fig. 1. The corresponding field derivatives are shown in Fig. 2. We find that the $\partial_z B_y$-component is actually the main contribution. It can be shown that the remaining components as well as side effects are either neglectable or can easily be dealt with [3,4].

4. Microfluidic separation system

The microfluidic structure chosen for the particle manipulation is shown in Fig. 3. The entrances (left) and the exits (right) are assumed to have a width of $80\mu m$.

The resulting fluid profile is obtained under the assumption of different entrance velocities at the upper v_1 and the lower entrance v_2, we write

$$v_1 = \xi_0 v_2 . \qquad (4.1)$$

For this particular geometry a relation factor of $\xi_0 = 1.4551$ is used. In that case, all liquid entering the geometry through the lower entrance leaves it through the lower exit, as well as this is the case for the upper part of the geometry. For this choice the geometry works as a hydrodynamic valve, where the flow direction is switched by the flow relation factor.

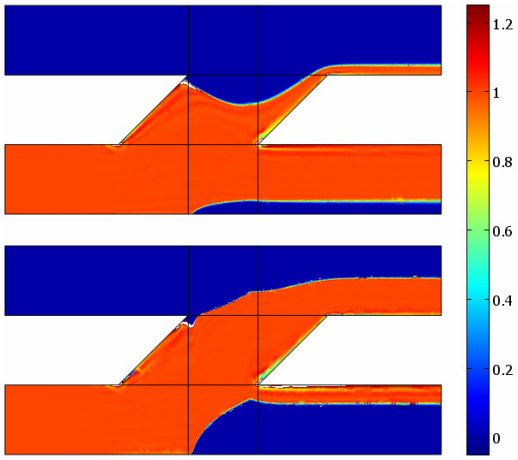

Fig. 4: Concentration profile for different particle sizes. In both cases particles with M_s = 1000kA/m migrate through an inhomogenous field with derivative $d_z H_y$ = 100kA/m^2. The particle radius is 0.5μm (upper picture) and 1.55μm (lower picture).

Applying a constant force along the central area of the geometry magnetic particles entering the geometry at a certain entrance can be dragged to the opposite exit. The particle behaviour depends on the particle properties, an example is shown in Fig. 4.

It can be shown [4], that the sensitivity can strongly be increased by adjusting different geometry parameters of the structure. Thus, this microfluidic structure is suitable as a separation device for magnetic particles in respect to different properties.

5. Experimental setup and sample preparation

5.1 Experimental setup

The experimental setup consist of an optical microscope with an attached CCD-camera and IC-socket that hold the sample. The microscope is an AXIOTECH VARIO carrying 3 EPIPLAN objectives (Zeiss, Germany) with magnification 20x, 50x, 100x and an 10x eyepiece. The self-made sample holder has an integrated IC-socket. All contacts of the IC-socket are connected to power supplies, measuring instruments and an analog-digital converter card in the computer. The CCD-camera M4+ CL (JAI, Japan) is mounted on top of the microscope and directly connected to a special video grabber card in the computer. The current through a conducting line can be measured and saved on the hard-disk together with the corresponding image and time. The described setup enables a measurement with 6 frames per second.

To ensure the absolute value of the magnetization to be comparable and the magentization orientation of the magentic beads to be out-of-plane perpendicular to the sample surface a homogeneous magnetic field in z-direction is needed. This is achieved by usage of a self-made cylindrical coil that can be attached to the sample holder. The magnetic field strength generated in the center of the coil is adjustable by the current through the wires. Here a field strength of 550 Oe is chosen which is the maximum of the described setup.

5.2 Magnetic beads

The magnetic beads have to satisfy some requirements. First, agglomeration of beads has to be supressed, because single magnetic beads, not clusters, are to be manipulated. Second, a high magnetic moment is needed for the manipulation of the magnetic beads (3.1).

For separation experiments superparamagnetic beads M-PVA SAV1 (Chemagen, Germany) were used. These beads have a size distribution from 0.5-1.5µm, which is sufficient for the optical detection of different beads sizes during flow experiments. A bead concentration of 0.25mg/ml was found to be suitable for the experiments.

5.3 Sample preparation

The sample is prepared in a two-step optical lithography process. First, the conducting lines represented in Fig.1 are structured onto a silicon substrate in a lift-off process. For this process the positive photoresist AR-P5350 (Allresist GmbH, Gemany) is used. After spin-coating the resist for 30s at 4000rpm the sample is heated to 85°C for 30 minutes. The lithography step itself is carried out with the DWL 66 (Heidelberg Instruments, Germany) laser lithography system.

The conducting lines are sputtered onto the substrate in a home-built sputter chamber that can hold up to six 2”sources and has a base pressure of 5x10^{-7}$mbar$. During the sputter process two metal layers are deposited. A 5nm

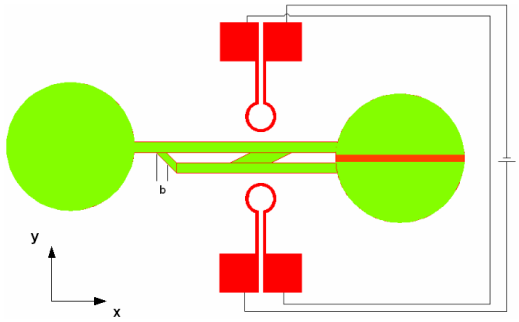

Fig. 5: Sketch of the channel design with conducting lines. The channel width is 80μm. By varying the geometry parameter b, the relation factor can be adjusted in a certain range.

tantalum layer is used as an adhesive layer which is afterwards coated with an 295nm gold layer. The lift-off with the remover AR 300-70 (All-resist GmbH, Germany) is carried out in an ultrasonic bath.

In the second lithography step, the fluidic channel is structured onto the substrate. The negative resist SU-8 25 (Microchem, USA) is used as channel material due to its excellent mechanical and chemical stability [5]. The resist is spinned onto the substrate for 30s at 2500rpm. Three baking steps are carried out. First, a soft-bake is applied (65°C for 5min, then 95°C for 15min). The sample is exposed with UV-light from a lithography system from THERMO ORIEL. The exposure dose is 270mJ. Afterwards the post exposure bake (65°C for 5min, then 95°C for 5min) is applied. After developing the sample with SU-8 developer (Microchem, USA), the final hard bake (150°C for 15min) is performed. A sketch of the final channel design can be seen in Fig. 5. Afterwards the samples are wire bonded into dual-in-line IC-packages.

For experiments the flow through micro-channels is generated by hydrostatic pressure only, so the realization of $\xi_0 = 1.4551$ is difficult. A simple approach is the control of the relation factor by varying the channel geometry, especially the geometry parameter b.

6. Experimental results

As a general remark according to the experimental results, it has to be noted that due to the shutter speed of the CCD-camera, beads appear in images as rods. This fact can be used to determine the position of the beads in z-direction. The flow profile is predicted to be parabolic in all dimensions, so the longest rods correspond to beads with maximum velocity and hence to beads at half channel level.

For evaluation of bead velocities the distance between rods in consecutive images is measured and the length of rods is taken into account to calculate the error. In order to analyze the effect of the geometry parameter b, velocities of beads at the same distance, with an accuracy of 1μm, to the channel walls in the upper and lower channel are compared. Simulations are carried out for comparison. The results are shown in Fig. 6. The experimental values for the dependence of the velocity ratio on the geometry parameter are in good agreement with theoretical predictions. The general characteristics are reproduced.

For separation experiments, the geometry parameter is chosen to be b = 60μm in order to generate a relation factor which is sufficient for experiments. Nevertheless, the condition without flux from the lower channel to the upper channel is not fulfilled and hence the force is applied in order to drag magnetic beads from the upper channel entrance to the lower channel exit. By using this direction of separation the influence of liquid flow from the lower channel entrance to the upper channel exit can be reduced to additional friction. The current through the conducting lines is limited to 184mA to prevent electromigration problems.

Results for the separation are shown in Fig. 7. Analysis of the images shows clearly the separation mechanism. It is furthermore discussed exemplarily, focusing again on magnetic beads at same distances to channel walls in the upper entrance with different sizes. The magnetic bead highlighted in Fig. 7a), b) has a diameter of 1μm. Manual tracking of the magnetic bead shows that it leaves the separation region through the upper channel exit. The analysis of the flow line of the magnetic bead in Fig. 7c), d) leads to a different result. The bead which is highlighted has a diameter of 1.5μm. Manual tracking shows in this case that the bead enters through the upper channel entrance and leaves the separation region through the lower channel exit.

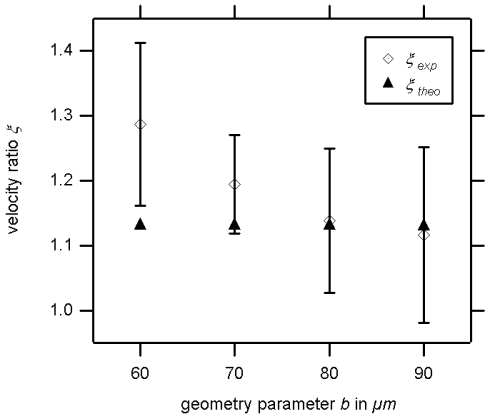

Fig.6: Dependence of velocity ratio on the geometry parameter *b*. The experimentally found dependence fits to theoretically predicted values.

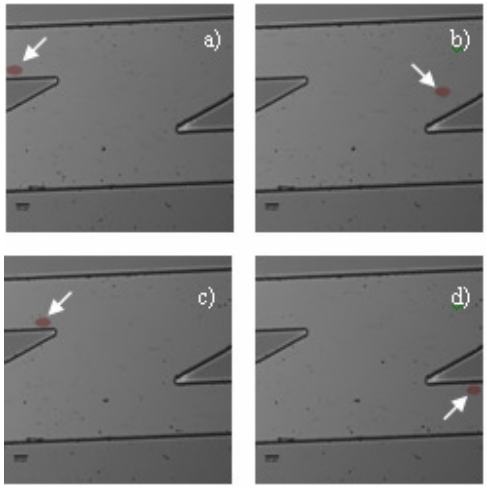

Fig.7: Images of the separation region, where a magnetic force in the direction of the lower part of the geometry is applied. The manually tracked beads are highlighted in red. a), b) A magnetic bead with diameter 1μm enters through the upper channel and leaves througth the upper channel exit. c), d) A magnetic bead with diameter 1.5μm entering the upper channel at the same distance to the channel walls as in a) leaves through the lower channel exit. The applied current through the conducting lines is 184mA and the homogeneous external field perpendicular to the sample surface has a field strength of 550Oe. The time-step between the images is 1020ms.

7. Conclusions

We have introduced a microfluidic structure, where magnetic microparticles are manipulated with a combination of hydrodynamic and electromagnetic forces. We experimentally proved that this structure is a suitable device to separate particles in respect to different properties e.g. size or magnetization. The experimental data show a very good agreement with the theoretical predictions.

8. References

[1] A. Hütten et al. New magnetic nanoparticles for biotechnology. *Jour. Biotech.* **112**, 47-63 (2004)

[2] M. Brezska et al. Detection and manipulation of biomolecules by magnetic carriers. *Jour. Biotech.* **112**, 25-33 (2004).

[3] F. Wittbracht, Mikrofluidisches Sortiersystem für magnetische Beads, *Bachelor thesis*, Bielefeld University (2007)

[4] A. Weddemann, Simulation des Bewegungszustandes magnetischer Partikel in Mikrokanälen, *Diploma thesis,* Bielefeld University (2006)

[5] C. Lin et al. A new fabrication process for ultra-thick microfluidic microstructures utilizing SU-8 photoresist. *J. Micromech. Microeng.* **12**, 590-597 (2002)

9. Acknowledgements

The authors would like to thank the BMBF "MrBead"-project and the SFB 613 for financial support.